

# DRAPING SIMULATION OF WOVEN FABRICS

*William R. Rodgers<sup>1</sup>, Xiaoshi Jin<sup>2</sup>, Jiang Zhu<sup>3</sup>, Terrence Wathen<sup>1</sup>,  
Mark Doroudian<sup>2</sup>, Venkat Aitharaju<sup>1</sup>*

*<sup>1</sup>General Motors Global Research and Development, Warren, MI, 48092*

*<sup>2</sup>ESI North America, Farmington Hills, MI, 48334*

*<sup>3</sup>Optimal CAE Inc., Plymouth, MI, 48170*

## Abstract

Woven fabric composites are extensively used in molding complex geometrical shapes due to their high conformability compared to other fabrics. Preforming is an important step in the overall process, where the two-dimensional fabric is draped to become the three-dimensional shape of the part prior to resin injection. During preforming, the orientation of the yarns may change significantly compared to the initial orientations. Accurate prediction of the yarn orientations after molding is important for evaluating the structural performance of the final part. This paper presents a systematic investigation of the angle changes during the preform operation for carbon fiber twill and satin weave fabrics. Preforming experiments were conducted using a truncated pyramid mold geometry designed and fabricated at the General Motors Research Laboratories. Predicted results for the yarn orientations were compared with experimental results and good agreement was observed.

## INTRODUCTION

The use of fiber reinforced composites as alternative to metallic materials for light weighting is gaining a significant amount of popularity in the automotive industry. This is due to their high specific stiffness, strength, and most importantly, their ability to manufacture complex shapes in a single operation. Composite manufacturing processes such as, resin transfer molding (RTM) and thermoplastic prepreg compression molding utilize the ability of these fabric based materials to drape [1-3] to assist in forming these complex shapes. During the draping process, the fabrics may undergo large changes in their microstructure due to scissoring and sliding. These changes in the microstructure of the preform are important to understand as they lead to changes in fabric properties such as permeability, fiber volume fraction, etc. These changes in fabric properties, in turn, need to be comprehended in order to correctly model the processing and performance of the final component.

Several different approaches have been reported in the literature to model the deformation characteristics based on several assumptions about the behavior of the fiber tows during the draping process. Van West et al., [4] developed a graphical simulation to describe the draping of a bi-directional fabrics over an arbitrary surface. They calculated the locations of the crossover points of the warp and weft fibers and from those the fiber angles and shear deformation of the fabrics were determined. Roberson et al., [5, 6] proposed the tow angle determination as analogous to a fisherman's net conforming to the part surface. They assumed the tows to be inextensible and connected at the knots at the intersection of warp and weft tows. The position of knots are determined by equations developed by Sickafus and Mackie [7]. Yu et al., [8] conducted characterization experiments for plain, five harness satin, eight harness satin, and

angle lock interweave woven fabrics made of carbon fiber. They showed that angle-lock interleave is relatively easy to deform in different modes, while the plain weave is difficult to deform and conform to part surfaces. Bergsma [9] conducted a simulation based on finite element analysis on the tows, modeling them as beams, connected at the cross over points. Tow stretching, tow buckling, and tow shear deformation were included. Good correlation results were reported with experiments.

Sidhu et al., [10] developed a finite element model considering the preform as 3-D truss elements and 3-D shell elements. In this work, the tows are modeled as bar elements and they are allowed to scissor and slide relative to one another. The inter-tow friction and friction angle jamming were modeled using shell elements. Good correlations with experimental results were reported for hemispherical stamping.

A small number of researchers modeled the meso-scale movement of textile composites using 3D hexagonal elements with displacements as a degree of freedom. Mathieu et al., [11] explained that the three-dimensional hyper-elastic constitutive law revealed a discrepancy and to remedy this he incorporated a rotational degree of freedom to the solid elements which resulted in improved correlations for three point bending and hemispherical forming experiments.

In the present work, material model 140, available in the PAM-FORM simulation tool, was used to model the draping behavior of twill woven (TC411) and 5-harness satin woven (SC685) fabrics. Fabric characterization experiments were conducted at the University of Tennessee for bending and shear stiffness. The bending experiments were carried out using Pierce cantilever beam equipment according to ASTM D1388. This evaluation was modeled and the experiments and model were found to be in good agreement. The results obtained from the shear stiffness evaluation suffered from many technical issues and therefore were not reproducible. For that reason, the shear modulus results were discarded and an inverse model was developed to provide the shear behavior. The material properties were validated through the use of experimental results generated using a truncated pyramid tool developed at the General Motors Research Laboratories with single ply fabrics. In the following sections, the details of the draping experiments and simulations that were conducted are presented. Based on the success of this work, it is hoped that the draping and the fiber angle changes observed during draping will be able to be predicted for more complex structures in the future.

## **EXPERIMENTAL – TRUNCATED PYRAMID TOOL**



### **Materials**

The details of the carbon fiber fabrics used in this study are provided in Table I. Both of the fabrics were received from Sigmatech High Technology Fabrics, Inc (Benicia, CA). The carbon fiber used to create these fabrics was T700SC-12000 carbon fiber (Torayca fiber from Toray Industries, Inc, Japan). The fabrics were cut with the machine (warp) direction defined as the 0° direction of the fabric. The fabric squares were cut using a Gerber Scientific model DCS2500 cutting table. For conducting the experiments using the GM Truncated Pyramid tool, the size of the cut fabrics was 508 mm x 508 mm. The fiber crossing angles of the twill and satin fabrics begins as 90°, in other words the weft (or fill) tows cross the warp tows at an angle of 90°. Although numerous orientations are possible for locating the fabric in the tool, we limited these experiments to the 0/90 global orientation.

## Tooling

A schematic drawing of the GM Truncated Pyramid tool used for these experiments is given in Figure 1 and an image of the tool used for the deformation of the fabrics is shown in Figure 2. The tool itself is made of cast acrylic resin. This allows the visual examination of the deformed fabrics while they remain in the tool. There is an aluminum frame used to support the lower half (cavity side) of the tool. As can be seen in Figure 2, a fixture can be fastened to the top half (core side) of the tool which allows the tool to be attached to an Instron model 5984 extra wide testing frame. This allows the deformation of the fabric to occur at a controlled rate.

Table I. Carbon Fabrics used in this study.

Fabric Designation	Areal Mass (g/m <sup>2</sup> )	Fabric Thickness (mm)	Type of Weave	Image
TC411	380	0.46 - 0.49	2 x 2 Twill	
SC685	385	0.52 - 0.55	5 Harness Satin	

## Deformation of the Fabrics

The fabrics were cut to 508 mm x 508 mm in the 0/90 global orientation. Care was taken during the cutting and placement operation to retain the original angles in the fabric. Following cutting, the fabric pieces were centered on the cavity side of the tool.

The fabrics were formed at a tool displacement rate of 25 mm/min. The test was designed to close at this speed while monitoring the load until a force of 5 KN was attained. During the deformation, the core of the tool deforms the fabric as it is being pushed into the cavity. Once a force of 5 KN was reached, the fixture was held at a constant closing distance for one minute. This allowed the force to decay somewhat. Following this the force was released and the tool was disconnected from the test frame while leaving the core side of the tool in place. No fiber movement was observed while removing the tool from the test frame. A representative curve from the deformation test is given in Figure 3.

Following the deformation, the entire tool was moved into the studio and photographed using high resolution digital imaging. Since the area of primary interest is the angled slope, care was taken to ensure the images were captured at 90° to this slope in order to minimize the chance for distortion in the measurement of the changed fiber angles. These images form the basis of the fiber angle measurements.

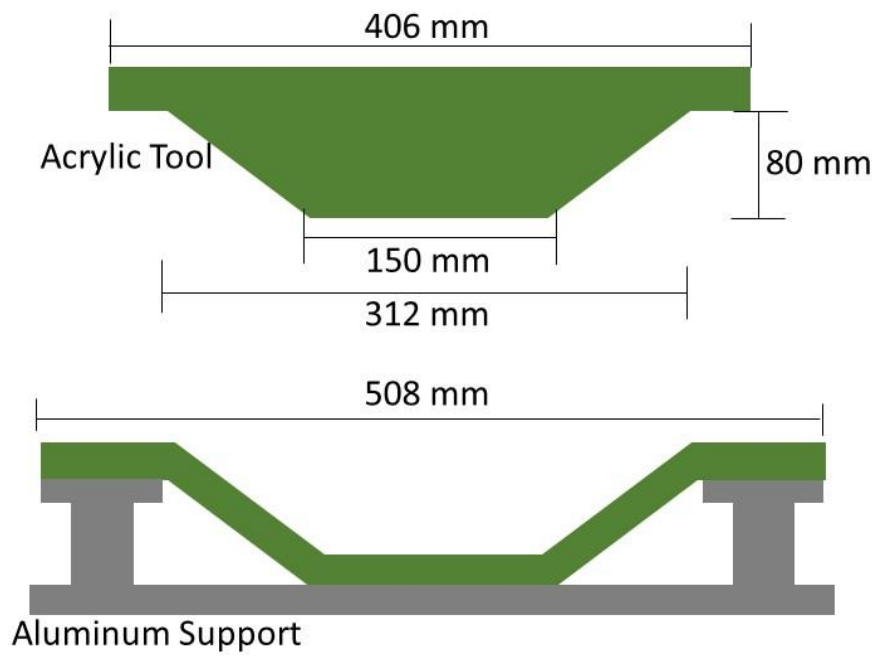


Figure 1. Schematic drawing of the truncated pyramid tool. Green is acrylic, Gray is aluminum (not to scale).

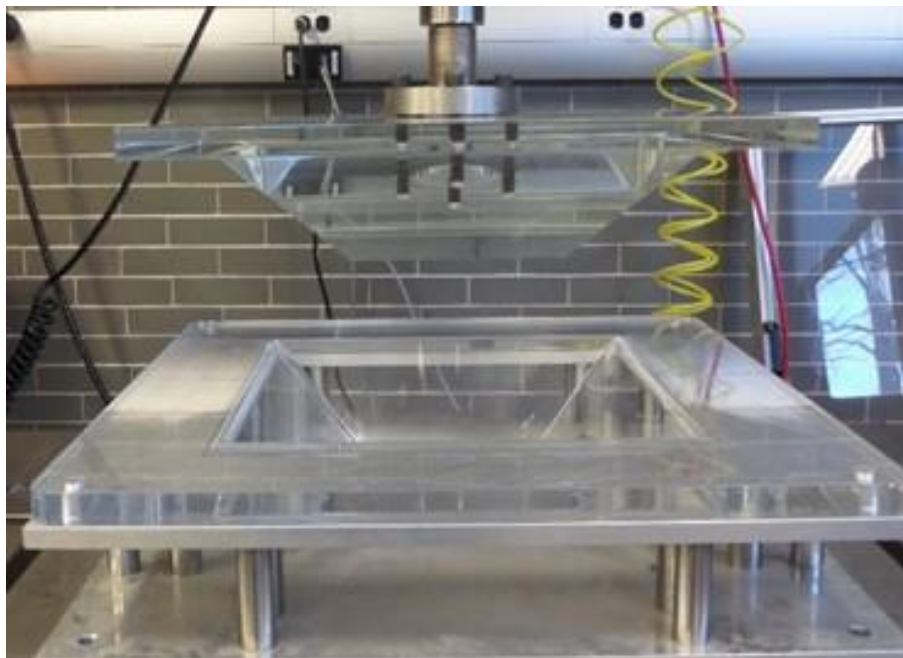


Figure 2. Image of the truncated pyramid tool

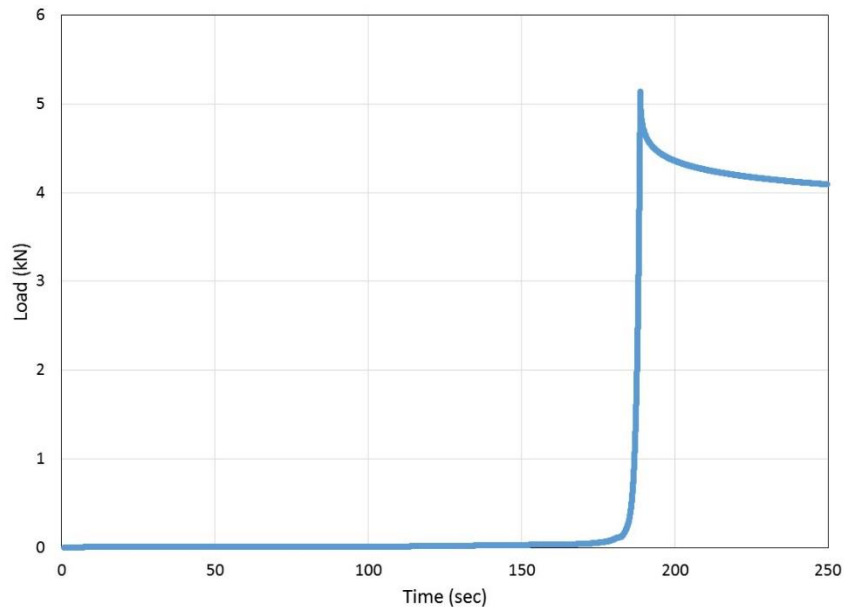


Figure 3. Load –displacement curve for the distortion of the twill fabric.

### Fiber angle measurements

Fiber angles were measured using an image analysis program, Image J, created by the National Institute of Health (<http://imagej.nih.gov/ij/>) [11]. The angle measurement tool allows the user to manually draw two intersecting lines and measures the included angle. Using this tool, angles were measured on the deformed fabric at multiple locations. In order to pin point which specific angles were measured in the image, a coordinate system was developed. For 0-90 fabric orientations, as shown in Figure 4, the warp fiber tows were numbered from left to right. For this particular image a total of 59 distinguishable warp tows were numbered. The weft fibers were identified alphabetically from top to bottom, starting with lower case letter and changing to upper case letter when it was necessary to repeat the letter use, a total of 33 weft tows were identified. Fiber angles were measured primarily at every 5x5 warp and weft intersection depending on the clarity and contrast of the image. If the image was not clear for a particular location that angle was not measured. Small yellow triangles were drawn on the image in order to identify the location where an angle measurement was taken. The angle was measured by drawing lines following the vertical edge of the warp tow and the other line following the center of the horizontal weft tow, as shown in Figure 5. The naming system for the angle consisted of combining the number of the warp fiber and the letter of the weft fiber. For example, the measured angle as indicated in Figure 5 below was designated as 25d.



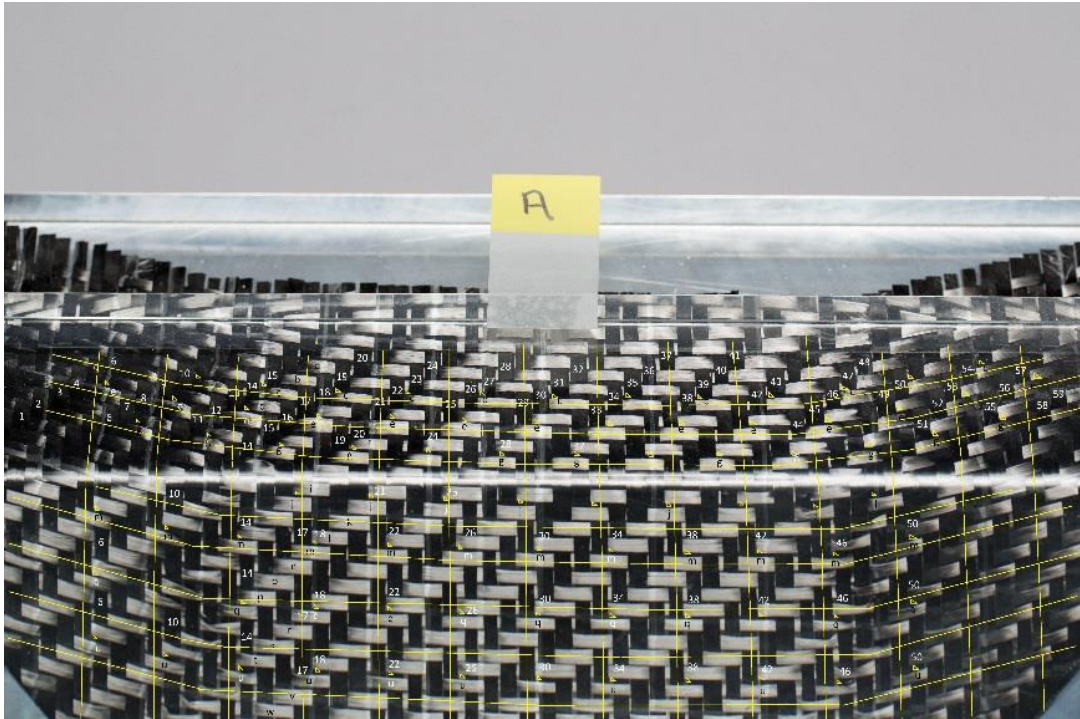


Figure 4. TC411, 2 x 2 Twill woven carbon fiber fabric

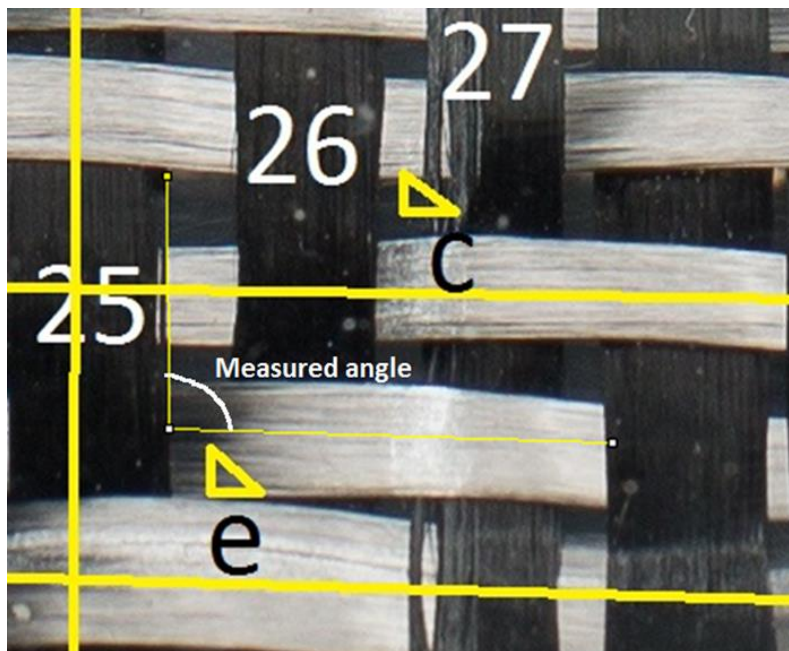


Figure 5. Image of fiber angle measurement using the Image J software.

## **Determination of the global location of the measurements**

The global location of each measurement was determined through the use of the coordinate system described above. Each image used for measurement included in it a 25.4 mm wide Post-it® tab (see Figure 4). Since this was a known width, it was used to calibrate the distances in the image. Using the line measurement tool, it was possible to determine the position of the measured angles in an X-Y coordinate system. Measurements taken from the edge of the deformed fabric to the tow on which the angles were being measured provided the Y coordinate. It was recognized that keeping the measurements to a single tow introduced some slight error into the position, but it was deemed to be a minor issue. The center of the tow in the middle of the fabric sheet was designated as the zero location for the X coordinate and the X coordinate was measured as the horizontal distance away from this centerline.

## **Error Control**

We recognized that error could be introduced into the measurements since this is a visual image analysis process. Therefore we determined an average error of the measurements by having two different operators carry out measurements of the angles. This resulted in a standard deviation of the measurements for the twill fabric being  $\pm 1.2^\circ$  and the standard deviation of the measurements for the satin fabric being  $\pm 1.7^\circ$ .

# **RESULTS AND DISCUSSION**

## **Material Data Calibration**

It is crucially important that a correct set of material properties is provided for the simulation of the forming process. Apart from the tensile modulus values in both warp and weft directions, two other major sets of material properties, assumed de-coupled from the tensile moduli in the composites material model MAT 140, are used in the simulation tool [12]. The first of these is the bending modulus. The bending modulus was evaluated for the two types of carbon woven fabrics. This was done through the use of the Pierce cantilever bending device according to ASTM D1388 at the University of Tennessee. The testing apparatus is shown in Figure 6.

Typically ASTM D1388 includes the measurement of the bending force to a fixed angle of  $41.5^\circ$  for the inclined surface, using a specimen size of 200 mm x 25 mm. The specimen is gradually moved across the edge of the top-surface until the leading edge of the fabric makes contact with the angled surface of the device, and then the overhang length is read from the included scale. Using  $41.5^\circ$  for the inclined angle is to simplify the calculations. However, we found that this inclined angle is far too large to be used for the woven carbon fabrics as they tend to be much stiffer than a usual fabric. For these materials, an inclined angle of  $16^\circ$  was found to provide reproducible results for these fabrics.



Figure 6. Pierce cantilever bending test device. Due to the stiffness of the woven carbon fabrics, the angle indicator is set to 16°.

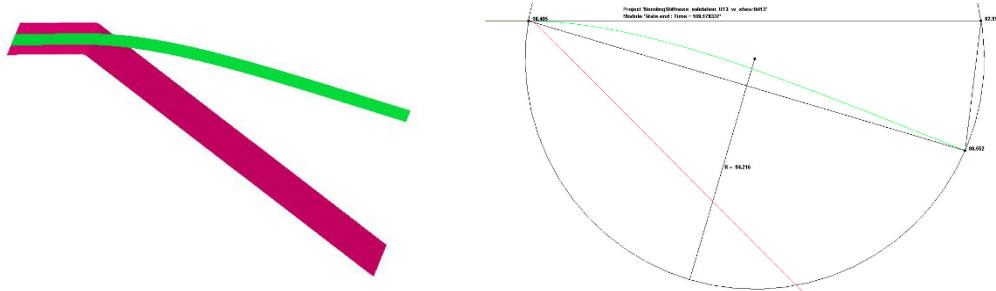


Figure 7. Simulation validation for calibration of the bending modulus values in Pierce cantilever bending tests.

Based on the scaling factor formula and the weighting factor according to the original work by Pierce [13], the measured overhang length data for both TC411 and SC685 woven carbon fabrics in two directions have been used to calibrate the bending moduli in the warp and weft directions, and then a simulation model was built to validate the bending modulus data as shown in Figure 7.

The resulting values from these calculations are shown in Table II. It was found that the simulation validation results with these bending modulus values for both fabrics closely match the experimental Pierce cantilever bending tests. Therefore we believe these values to be acceptable.

The second data set required for good simulation is the shear behavior of the fabric. This parameter is also de-coupled in the material model used for the simulation. Since the data from our picture frame tests were unusable, we had to turn to another method to obtain the shear information that was required.



Table II. Calibrated bending modulus values based on Pierce test with 16° inclining angle

	SC685 Warp	SC685 Weft	TC411 Warp	TC411 Weft
Average Overhang Length (mm)	187.2 ± 2.5	162.6 ± 2.1	192.3 ± 1.4	184.1 ± 4.1
Flexural rigidity (N·m)	1.87x10 <sup>-2</sup>	1.22x10 <sup>-2</sup>	2.03x10 <sup>-2</sup>	1.77x10 <sup>-2</sup>
Bending modulus (GPa)	2.25	1.39	2.34	2.04
Incline angle calculated from simulation (°)	16.0	16.1	16.1	16.0

From the literature covering the shear behavior of fabrics, we can be reasonably certain of two noticeable factors:

1. The shear modulus is not a constant
2. The initial shear modulus is very small

Further evaluation of the literature on the shear behavior of woven fabrics indicated that the fabric shear is initially due to the friction between the warp and weft tows, and after the gaps between tows close, the lateral compression becomes the dominating factor for the shear, making the shear modulus increase rapidly. In order to comprehend this behavior in the model, the following shear modulus model has been used for narrowing down the shear stiffness behavior, (see Figure 8).

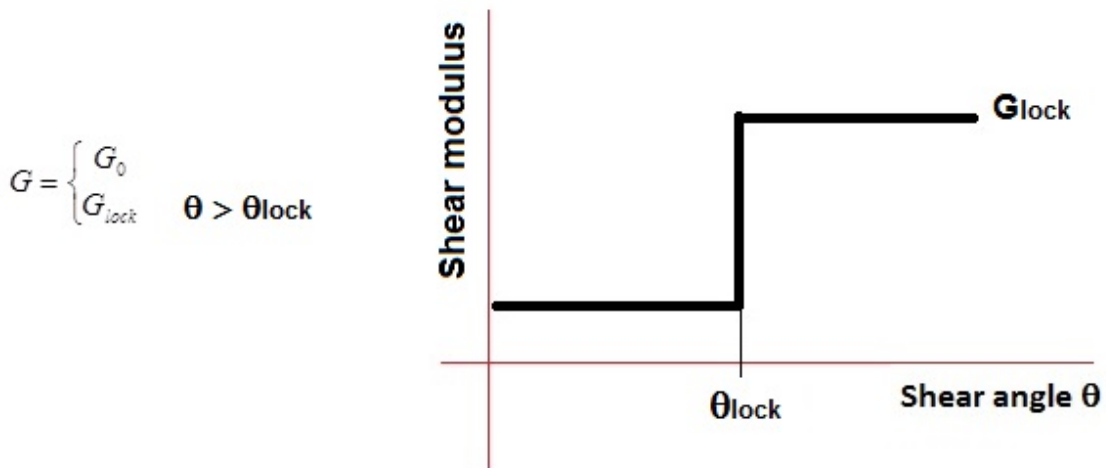


Figure 8. Shear modulus models used in simulation

## Simulation using Inverse Analysis

Although calibration of the bending moduli based on the experimental evidence was done. In practice, the shear behavior still needed to be determined. Therefore, we turned to an inverse analysis model to provide the correct set of the material properties to be used in the simulation. The goal of this inverse analysis was to match the experimental results from the forming process. Therefore the inverse analysis model can be described as follows:

$$\text{Minimize } f(G_{init}, \theta_{lock}, G_{lock}) = \sum_i \left\{ \left[ \frac{A_i^s(G_{init}, \theta_{lock}, G_{lock}) - A_i^m}{A_{max}^m} \right]^2 \right\} \quad (1)$$

where  $A_i^s$  for the shear angle predicted by simulation at the  $i$ th location,  $A_i^m$  for the shear angle measured at the  $i$ th location,  $A_{max}^m$  the maximum shear angle measured,  $G_{init}$  the initial shear modulus,  $\theta_{lock}$  the locking angle, and  $G_{lock}$  the shear locking modulus. The constraint set is:

$$\begin{aligned} 4^\circ &\leq \theta_{lock} \leq 18^\circ \\ 0.001GPa &\leq G_{init} \leq 0.5GPa \\ 0.5GPa &\leq G_{lock} \leq 4.0GPa \end{aligned} \quad (2)$$

Since there are only a finite number of measurement locations, the above described problem could be solved with an optimization algorithm. Although the shear behavior can be described with a quite complex model and it can be described as a look up table in the simulation tool, if a mathematical form of it cannot be explicitly described, there would be many design variables in the optimization model. It can be seen that a simplified shear behavior model with just three parameters, such as the constant model with an initial shear modulus, a locking angle, a shear lock modulus, are used in the inverse model. On the other hand, the inverse analysis model can be solved with a Design of Experiments (DOE) approach for a reduced number of variables to vary within their corresponding available ranges, and a certain path for the variations can be achieved without running a full set of combinations.

## Measurement of the Twill Fabric (TC411)

Figure 9 shows the force vs time curve for the deformation of the twill fabric with the force axis greatly expanded. At this scale it is clear that at the start of the deformation, very little force is required in order to have the fabric be deformed into the tool. However, the force is increasing linearly.

At roughly the half-way point of the total deformation (112 seconds, 47 mm), the slope of the line changes to a higher value, indicating that it is taking somewhat more force to continue to deform the fabric. This corresponds to the point in the test where the fabric is no longer only being bent due to the action of the core side of the tool but is beginning to be drawn into the cavity.

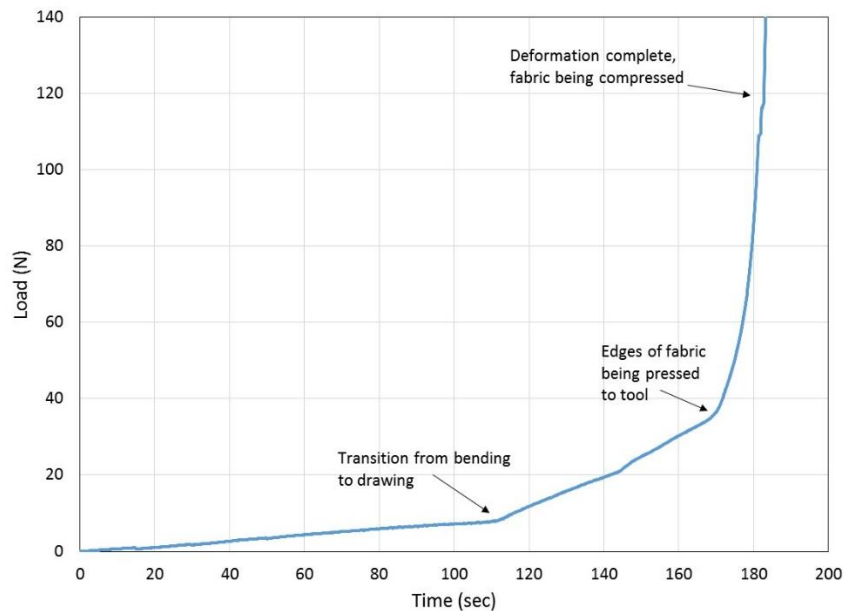


Figure 9. Load vs Time Curve for the deformation of the 2 x 2 twill fabric.

The next change in slope happens when the fabric has essentially filled the tool (~ 170 s, ~ 70 mm), and the final angle changes begin. At this point the top of the fabric is being flattened by the core side of the tool.

The final slope change happens after roughly 183 s and the deformation is essentially complete with the force reaching the 5 KN limit at 189 s while the fabric is compressed.

### Comparison of Overall Draw-in for TC411

Figure 10 is an image taken of the global fabric distortion. It is clear from the image that the center part of the edges of the fabric draw in more than the corners of the fabric in the 0/90 global orientation. This is a completely understandable and reasonable result as 30 mm is half the difference between the length of the fabric (508 mm) and the deformed line length in the middle of the tool (568 mm). This draw in happens on all four sides of the fabric.

When this draw in of the fabric is simulated, a draw in of 30 mm in the center of the fabric (as shown in Figure 10) also results, and the simulation also provides the correct overall shape. From these results, it is clear that this draw in can be simulated through the use of PAM-FORM. This is a simple case, however it does provide evidence that the system may be able to be modeled.

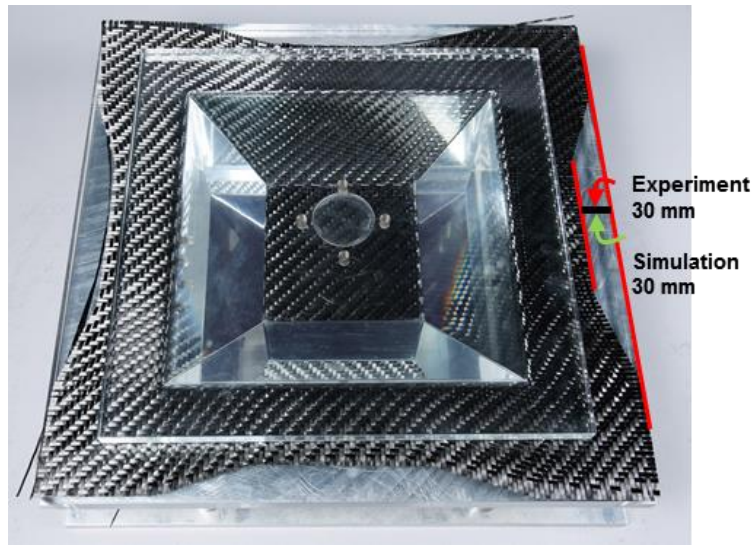


Figure 10. Global view of TC411 fabric following deformation

### Measured Angle Change for TC411

Figure 11 shows the change in the shear angle vs distance from the centerline for the fiber that was 59 mm from the edge of the fabric (fiber m) at the start of the test. The insert in the upper right of the figure shows the approximate position of the fiber line that was used to generate the figure. The white line in the image marks the edge of the 45° slope in the tool. There are two sets of measurements shown on the chart. These were obtained from two different researchers measuring the angles independently. Since each angle was measured in the same orientation, shear angle changes that happen on the negative side of the centerline show a positive shear angle, and changes on the positive side of the centerline exhibit negative shear angles. Due to the focus of the image, certain areas of the image could not be used for angle measurement.

As a general rule, the shear angle changes were greater on the sides of the part. This corresponds to where the overall length of line for the deformed material is increasing as the point of interest moves closer to center of the tool. Eventually, moving toward the center of the tool, the deformed line length stabilizes and the angle changes approach zero. Since the tool is symmetrical, the same thing happens on the other side of center.

The maximum shear angle measured for this fabric at this fiber tow is 14.4° at roughly 105 mm from center. After this the shear angle change decreases slightly. The shear angle changes are near zero in the middle of the tool where the deformed line length remains a constant (vertical lines on the graph define this region.) The deformed line length begins to change again on the other side of the tool and the shear angles again take on a value.

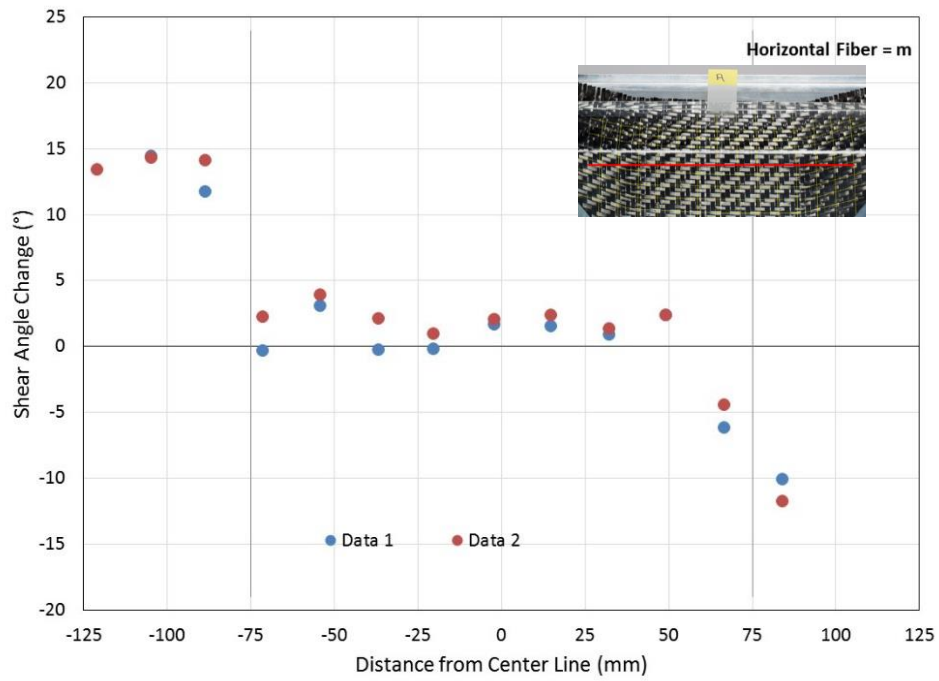


Figure 11. Fiber angle change for fiber 'm' for the TC411 fabric

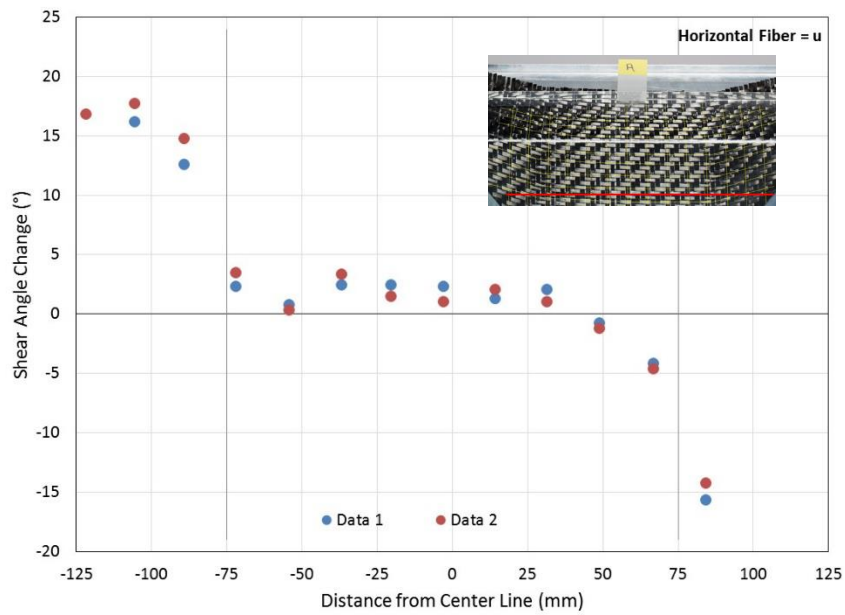


Figure 12. Fiber angle change for fiber 'u' with the TC411 fabric.

The same behavior is observed with a fiber that was further from the edge of the fabric. Figure 12 shows the shear angle behavior for a fiber that started out 90 mm from the edge of the fabric (fiber u). The maximum shear angle change observed at this location is 17.7°. So further down the sides of the tool the shear angle changes are higher, but not greatly so.

### Comparison of Simulated Angle Change with Experimental Results for TC411 Fabric

The parameters used to simulate the experimental results for the TC411 fabric in the 0/90 global orientation are provided in Table III. The comparison of the results of the shear angles changes between the experimental measurements and the simulated values from the model are shown graphically in Figures 13 and 14 and presented in table form in Appendix A (Tables A1 and A2). Although the percentage differences between the simulated values and the experimentally measured values can be rather large (~ 35%), this only happens near the corner of the tool, with the majority of the results being within 15% of the experimentally measured values.

Table III. Simulation Parameters for the TC411 Twill Fabric

Parameter	Value
$G_{initial}$	0.005 GPa
$\theta_{lock}$	4°
$G_{lock}$	1.5 GPa

Looking at the details of the comparison, shape of the shear angle change simulation matches well with the measured results, i.e. the angle changes of the fibers at the extreme edges of the fabric decrease slightly from the values slightly in from the edge. The simulation also accurately captures where the shear angle changes tend to return to zero in the middle of the deformation. Therefore, it is clear that the simulation is capable of providing a reasonable fit to the experimentally measured shear angles.



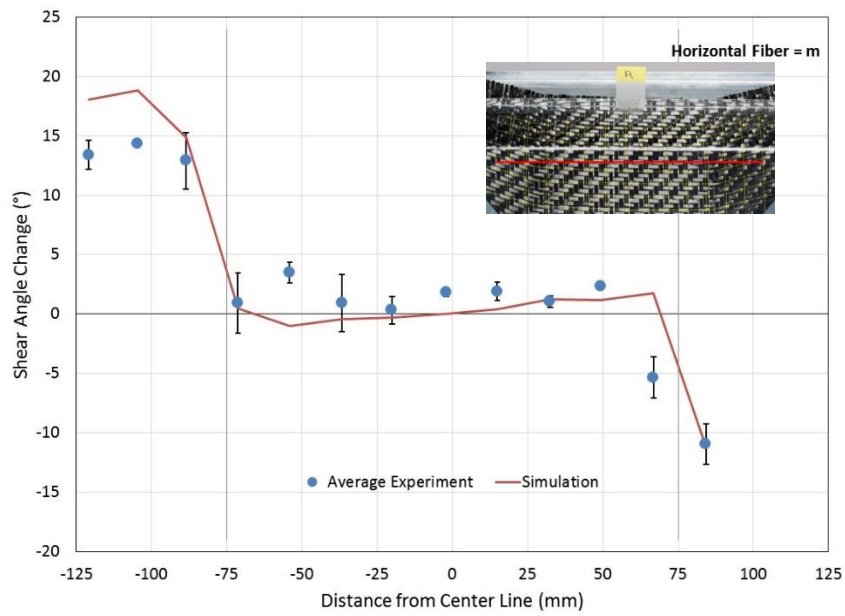


Figure 13. Simulation results for the shear angle change along fiber "m" for the TC411 twill fabric.

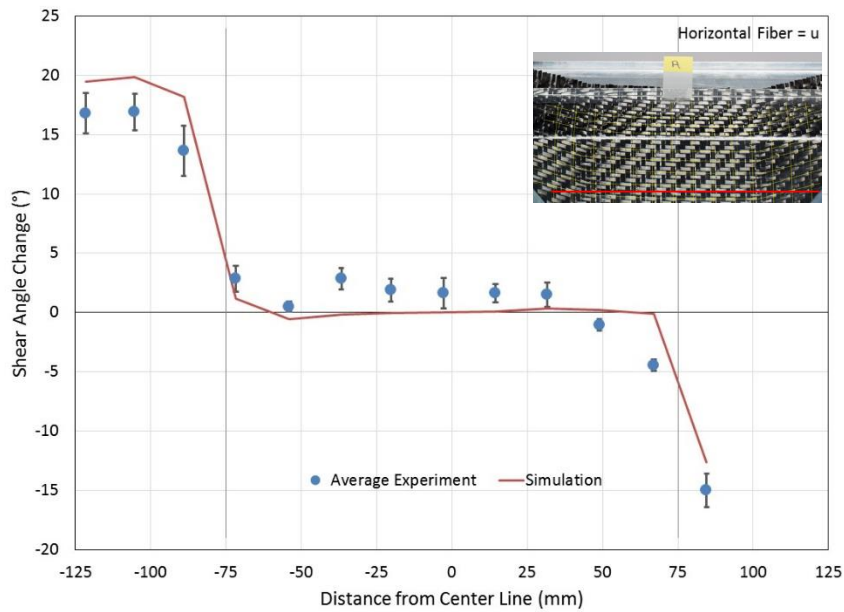


Figure 14. Simulation results for the shear angle change along fiber "u" for the TC411 twill fabric.

## Measurement of the Satin Fabric (SC685)

Figure 15 shows the force vs time curve for the deformation of the SC685 satin fabric with the force axis greatly expanded. As previously observed with the TC411 fabric, little force is required at the start of the deformation. The satin fabric follows the same sequence of steps as that observed for the twill fabric. The forces for the satin however, are slightly lower, 6.3 N at the initial change in curvature as opposed to 8.1 N for the twill fabric. At the second change in curvature, the forces are 35 N versus 37 N for the satin and twill fabrics respectively. This is the case for the entire curve.

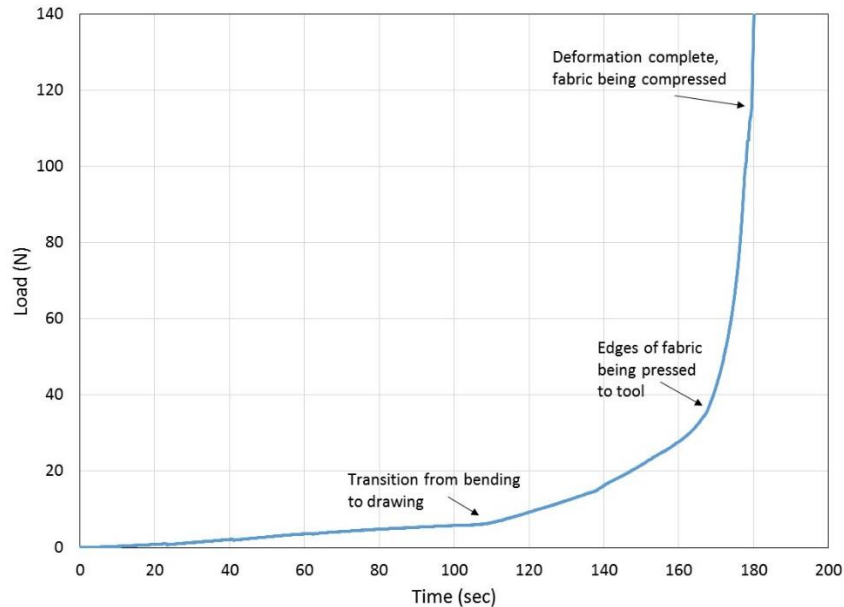


Figure 15. Load vs Time curve for the deformation of the SC685 satin fabric.

Figure 16 shows the shear angle change vs. distance from the center line at fiber “p” for the SC685 satin fabric. As with the figures associated with the TC411 fabric, the insert in the upper right corner of the figure shows the approximate location of the fiber used to generate the figure. In this case, fiber “p” was 62 mm from the edge of the fabric at the start of the test. The differences in the measurements are from two different investigators measuring the same images (represented as Data 1 and Data 2). As observed with the TC411 fabric, the fiber angles changed more significantly on the edge of the fabric than the center area. The maximum observed shear angle change is  $11.1^\circ$  at 92 mm from the center. For the center area of the fabric, from -75 mm to 75 mm, there is very little change observed in shear angle. The maximum change in the center area is only  $3.2^\circ$ .

Figure 17 shows the shear angle change vs. distance from the center line at fiber “z” in the SC685 satin fabric. The position of this fiber is further down the slope of the surface (92 mm from the edge of the fabric). The trend in shear angle change is the same as for fiber “p” with significant changes on the edge of the fabric and little change in the center area. For fiber “z”, the maximum fiber angle change is  $16.6^\circ$  at 129 mm. The maximum shear angle change in the center area, from -75 mm to 75 mm is  $4.2^\circ$  nearly the same as that observed for fiber “p”.

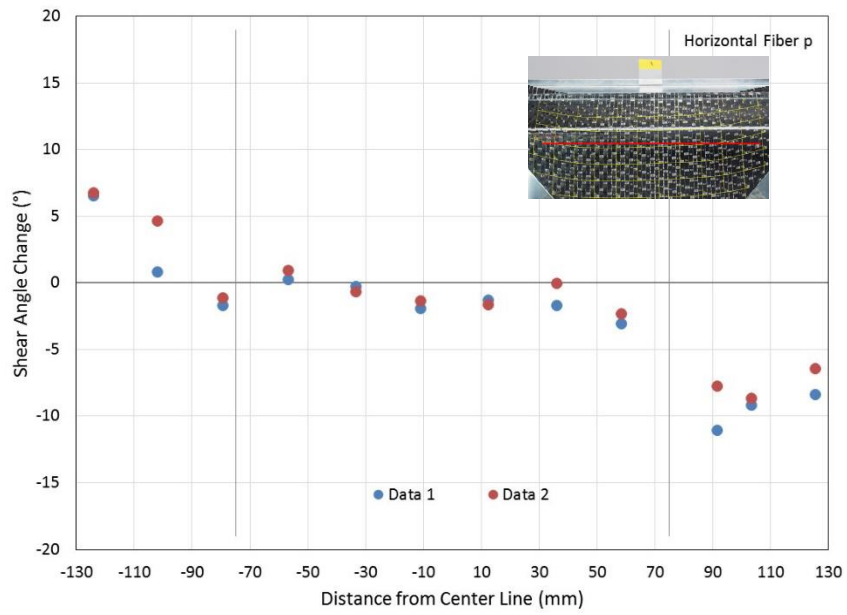


Figure 16. Fiber angle change for fiber 'p' with the SC685 fabric.

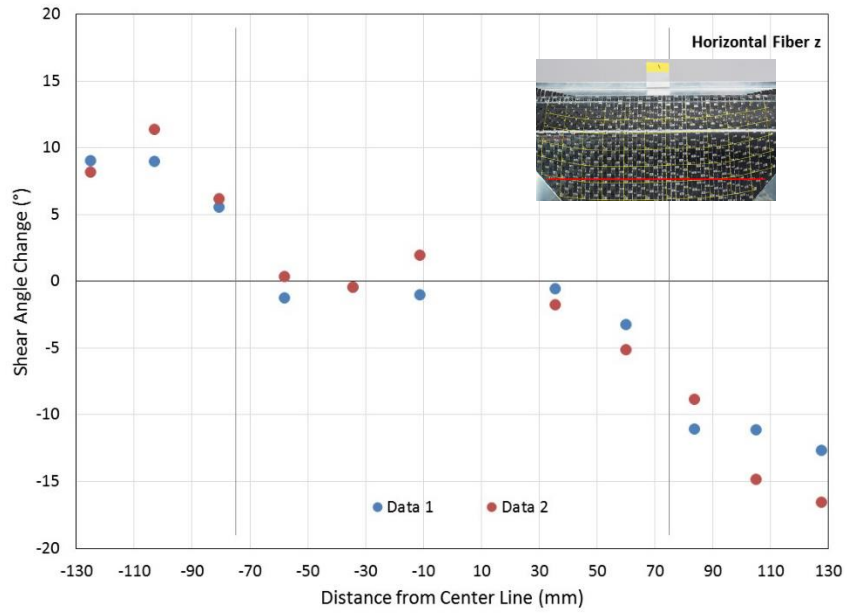


Figure 17. Fiber angle change for fiber 'z' with the SC685 fabric.

The maximum shear angle change for fiber “p” is 11.1° while for fiber z it is 16.6°. It is also interesting to note that the fiber angle changes for fiber “p” appear to be symmetrical, while the measurements for fiber “z” appear to be somewhat skewed; with the fibers on one side of the image having a larger fiber angle change than those on the other side. The reason for this difference is not yet clear, however, considering the differences in the measurements between the two investigators, it is difficult to determine whether the change in Y position from fiber “p” to fiber “z” has any real effect on the shear angle changes.

### Comparison of the Simulated Angle Change with Experimental Results for SC685 Satin Fabric

The parameters used to simulate the experimental results for the SC685 fabric in the 0/90 global orientation are provided in Table IV. The comparison of the results of the shear angles changes between the experimental measurements and the simulated values from the model are shown graphically in Figures 18 and 19 and are presented in table form in Appendix A (Tables A3 and A4). It is clear from looking at the simulated data that the simulation of the SC685 fabric is not as accurate as that observed with the TC411 fabric.

Table IV. Simulation Parameters for SC685 Satin Fabric

Parameter	Value
$G_{initial}$	0.4 GPa
$\theta_{lock}$	6°
$G_{lock}$	1.5 GPa

The general shape of the simulated results, higher angle changes near the edges of the fabric and near zero angle change in the center of the fabric follows the same trend as observed with the experimental measurements and with the TC411 fabric. The simulated angle changes for fiber “p” follow the general shape appropriately, however, they are of a higher magnitude.

The simulated angle changes for fiber “z” are also larger than the experimentally measured magnitude. However, the angle changes on the positive side of the center line, (from 0 to 130 mm) match more closely than the angle changes on the negative side of the center line (from -130 to 0 mm). This indicates that the two sides of the fabric did not perform in the same manner.

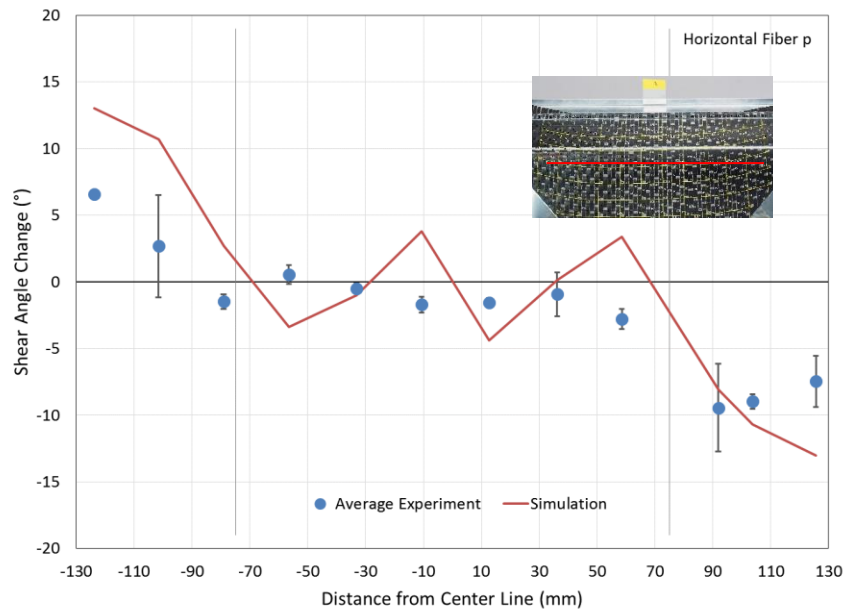


Figure 18. Simulation results for the shear angle change along fiber “p” for the SC685 satin fabric.

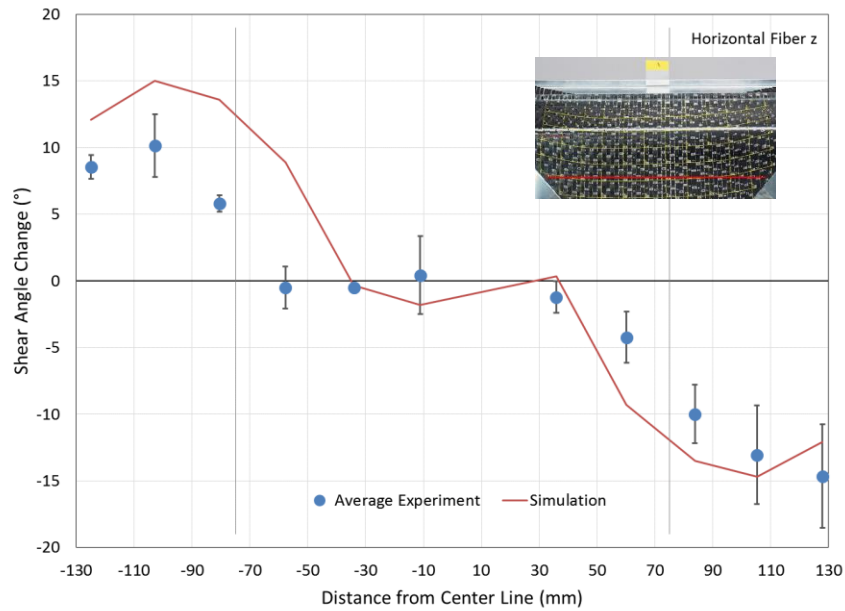


Figure 19. Simulation results for the shear angle change along fiber “z” for the SC685 satin fabric.

Examining the image used to analyze the fiber angle changes for this fabric, there are a few anomalies that should be noted. The first is that there is evidence of buckling in some of the fibers

on the negative side of the centerline (see Figure 20). It is possible that this allowed the fiber angles to change during the experiment thus leading to values that are different than those arrived at during the simulation. It is also clear from Figure 20, that the weft fibers with the SC685 satin fabric have become narrower during the experiment while the warp fibers remained at their original width. In the undeformed fabric, the fibers in the warp and weft directions of the SC685 fabric have measured widths of  $3.4 \pm 0.4$  mm. In the deformed fabric, the warp fibers retain their width ( $3.8 \pm 0.3$  mm) while the weft fibers become significantly narrower ( $2.4 \pm 0.2$  mm). It is possible that this change in the fiber width would affect the friction between the fibers leading to lower angles being observed in the experiment than those that were determined during the simulation, or that another deformation mechanism was involved with this particular fabric that was not taken into account in the simulation.

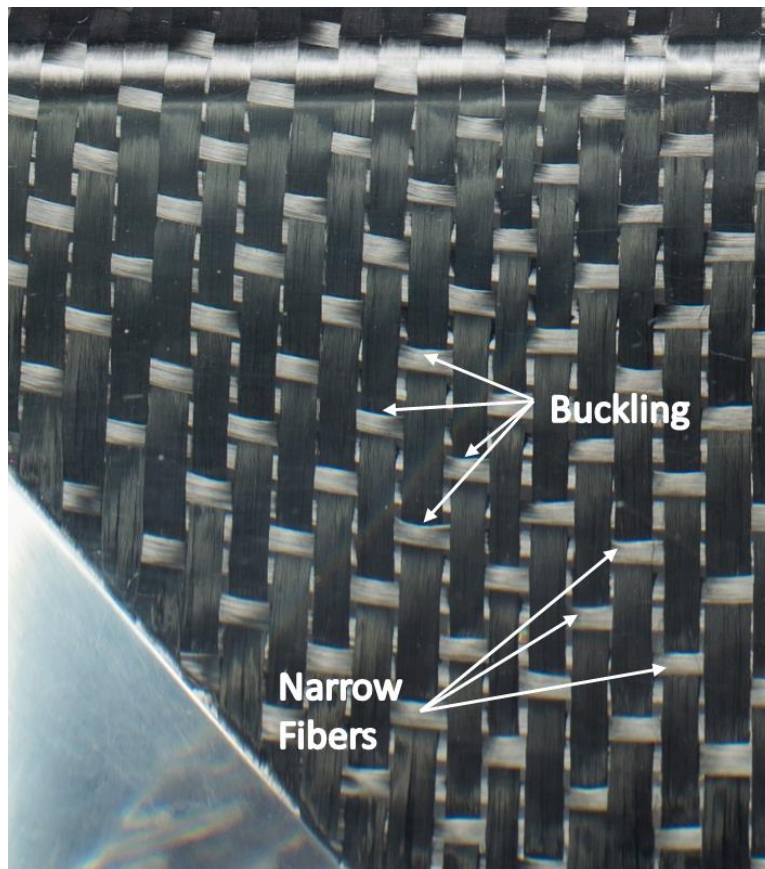


Figure 20. Image of the left side of SC685 satin fabric showing anomalies.

### Summary and Next Steps

Although a simulation tool for preforming is readily available, understanding the material property and process condition sets are crucial for correctly modeling the behavior of woven carbon fabrics during the manufacturing process. This paper presents work aimed at combining experimental measurements and computational models to determine the set of material properties that lead to proper simulation of the behavior of woven carbon fabrics during forming.



While the current performance of the simulation tool for the TC411 twill woven fabric matches well with experimental evidence; for the SC685 5-harness satin woven material, further work is necessary in order to account for the fabric behavior that was observed during the experimental deformation study.

This future work will involve a second attempt at capturing the shear modulus parameters through the use of a picture-frame test. This will help define the appropriate parameters for the simulation of this fabric. Also, while simulations and measurements have been carried out in the 0/90 global orientation, it is still necessary to evaluate the simulations for the results when the fabric is in a 45/-45 global orientation. These simulations will provide a good confirmation of the material properties that have been inversely determined in this work.

Additionally, in these experiments, the boundary conditions were all free, i.e. none of the edges were fixed in space. Further work should also include simulating the fiber angle changes when one side of the fabric is captured and is not allowed to draw in. This will provide needed information on a potentially real scenario that could develop when this system is used in actual applications.

## **Acknowledgements**

The information, data, or work presented herein was funded in part by the Office of Energy Efficiency and Renewable Energy (EERE), U.S. Department of Energy, under Award Number DE-EE0006826. The information, data, or work presented herein was funded in part by an agency of the United States Government. Neither the United States Government nor any agency thereof, nor any of their employees, makes any warranty, express or implied, or assumes any legal liability or responsibility for the accuracy, completeness, or usefulness of any information, apparatus, product, or process disclosed, or represents that its use would not infringe privately owned rights. Reference herein to any specific commercial product, process, or service by trade name, trademark, manufacturer, or otherwise does not necessarily constitute or imply its endorsement, recommendation, or favoring by the United States Government or any agency thereof. The views and opinions of authors expressed herein do not necessarily state or reflect those of the United States Government or any agency thereof.

## **Bibliography**

1. Bickerson, S., Simacek, P., Guglielmi, S.E., and Advani, S.G., "Investigation of draping and its effects on the mold filling process during manufacturing of curved composite parts," *Composites, Part A*, 28A, 1997, pp 801-816.
2. Li, H., Gutowski, "The forming of thermoset composites," *Composites sheet forming, Composites Material Series, Vol 11*, Elsevier, 1997, pp 441-471.
3. Long, A.C., Blanchard, P.U., Rudd, C.D., and Smith, P., "The development of integrated process model for liquid composite moulding," *Composites, Part A, Vol 29A*, 1998, pp 847-854.
4. Van West, B.P., Pipes, R.B., and Keefe, M., "A simulation of the draping of bidirectional fabrics over arbitrary surfaces," *J. Textile Institute, Vol 81, No. 4*, 1990, pp 448-460.
5. Robertson, R.E., Hsiue, E.S., and Yeh, G.S.Y., "Continuous fiber rearrangements during the molding of fiber composites I. Flat cloth to hemisphere," *Polymer Composites, Vol 2, No 3*, July 1981, pp 126-131.

6. Robertson, R.E., Hsiue, E.S., and Yeh, G.S.Y., "Continuous fiber rearrangements during the molding of fiber composites II. Flat cloth to a rounded cone," *Polymer Composites*, Vol 5, No 3, July 1984, pp 191-197.
7. Sickafus, E.N., Mackie, N.A., "Interstitial space in hardsphere clusters," *Acta Crystallographica Section A*, Volume 30, Issue 6, 1974, Pages 685–874.
8. Yu, J.Z., Cai, Z., Ko, F.K., "Formability of textile preforms for composite applications. Part 1: Characterization experiments", *Composite Manufacturing*, Vol 5, No 2, 1994, pp 113-122.
9. Bergsma, O., "Computer simulation of 3D forming process of fabric reinforced plastics," *Proceedings of the Ninth International conference on Composite Materials (IICM/9) Madrid July 12-16, 1993*, pp 560-567.
10. Sidhu, R.M.J.S., Averill, R.C., Riaz, M., and Pourboughrat, F., "Finite element analysis of textile composite preform stamping," *Composite Structures*, Vol 52, 2001, pp 483-497.
11. Schneider, C.A., Rasband, W.S., Eliceiri, K.W. "NIH Image to ImageJ: 25 years of image analysis". *Nature Methods* 9, 2012, pp 671-675.
12. Model Calibration, Composites material model 140 for draping simulation, Pam-Form 2G manual
13. Pierce, F.T., "The "handle" of cloth as a measureable quantity," *J. Textile Inst Trans*, (1930), 21: T377-416.

## APPENDIX A – Tabulated Test Results

Table A1. Results of Measured and Simulated Shear Angle Change for Fabric TC411 (2x2 Twill) Fiber “m”.

Y-Position (mm)	X Position (mm)	Average Experimental Shear Angle Change (°)	Simulated Shear Angle Change (°)
59.1	-120.9	13.4 ± 1.2	18.1
59.1	-104.5	14.3 ± 0.1	18.8
59.1	-88.5	12.9 ± 2.4	14.9
59.1	-71.3	0.9 ± 2.6	0.4
59.1	-54.1	3.5 ± 0.9	-1.0
59.1	-36.7	0.9 ± 2.4	-0.5
59.1	-20.1	0.3 ± 1.2	-0.3
59.1	-2.1	1.8 ± 0.4	0.0
59.1	14.9	1.9 ± 0.8	0.4
59.1	32.5	1.1 ± 0.5	1.3
59.1	29.3	2.3 ± 1.7	1.2
59.1	66.9	-5.4 ± 1.7	1.8
59.1	84.3	-11.0 ± 1.7	-11.1

Table A2. Results of Measured and Simulated Shear Angle Change for Fabric TC411 (2x2 Twill) Fiber “u”.

Y-Position (mm)	X Position (mm)	Average Experimental Shear Angle Change (°)	Simulated Shear Angle Change (°)
89.6	-121.6	16.8 ± 1.7	19.5
89.6	-105.3	16.9 ± 1.5	19.8
89.6	-89.0	13.6 ± 2.1	18.2
89.6	-71.1	2.8 ± 1.1	1.2
89.6	-54.0	0.5 ± 0.4	-0.6
89.6	-36.7	2.9 ± 0.9	-0.2
89.6	-20.3	1.9 ± 1.0	-0.1
89.6	-2.7	1.6 ± 1.3	0.0
89.6	14.5	1.6 ± 0.8	0.1
89.6	31.7	1.5 ± 1.0	0.3
89.6	49.0	-1.1 ± 0.5	0.2
89.6	67.0	-4.5 ± 0.5	-0.1
89.6	84.6	-15.0 ± 1.4	-12.7

Table A3. Results of Measured and Simulated Shear Angle Change for Fabric SC685 (5-harness Satin) Fiber “p”.

Y-Position (mm)	X Position (mm)	Average Experimental Shear Angle Change (°)	Simulated Shear Angle Change (°)
62	-123.7	6.6 ± 0.2	13.0
62	-101.6	2.7 ± 3.8	10.7
62	-79.1	-1.5 ± 0.5	2.7
62	-56.5	0.6 ± 0.7	-3.4
62	-33.2	-0.5 ± 0.4	-1.0
62	-10.6	-1.7 ± 0.6	3.8
62	12.7	-1.5 ± 0.3	-4.4
62	36.2	-0.9 ± 1.7	0.16
62	58.6	-2.8 ± 0.8	3.4
62	91.9	-9.4 ± 3.3	-8.1
62	103.7	-9.0 ± 0.5	-10.7
62	125.7	-7.5 ± 1.9	-13.0

Table A4. Results of Measured and Simulated Shear Angle Change for Fabric SC685 (5-harness Satin) Fiber “z”.

Y-Position (mm)	X Position (mm)	Average Experimental Shear Angle Change (°)	Simulated Shear Angle Change (°)
91.5	-124.9	8.5 ± 0.9	12.1
91.5	-102.8	10.1 ± 2.3	15.0
91.5	-80.5	5.8 ± 0.6	13.6
91.5	-57.7	-0.5 ± 1.6	8.9
91.5	-34.0	-0.5 ± 0.0	-0.32
91.5	-11.1	0.4 ± 2.9	-1.8
91.5	35.9	-1.2 ± 1.2	0.33
91.5	60.2	-4.2 ± 1.9	-9.3
91.5	83.8	-10.0 ± 2.2	-13.5
91.5	105.3	-13.0 ± 3.7	-14.7
91.5	127.9	-14.7 ± 3.9	-12.1